JOURNAL OF MATERIALS SCIENCE 31 (1996) 1065–1070

The effect of indentation-induced cracking on the apparent microhardness

HONG LI
Battelle Pacific Northwest Laboratories, Richland, WA 99352, USA
R. C. BRADT*
Department of Metallurgical and Materials Engineering, University of Alabama, Tuscaloosa, AL 35487-0202, USA

The phenomenon of apparent microhardness increase with increasing applied indentation test load, the reverse indentation size effect (RISE), was addressed from the viewpoint of indentation-induced cracking. The apparent microhardness when the cracking occurs was found to be related to the applied indentation test load as $P^{5/3}$. Previously published results on single crystals of silicon, GaAs, GaP and InP, which differ by a factor of four, all fall on the same line when analysed through this concept. It is concluded that the RISE is a result of the specimen cracking during the indentation.

1. Introduction

For the measurement of the indentation microhardness of solids, there exists a dependence of the apparent microhardness on the applied test load. This phenomenon is known as the indentation size effect, frequently abbreviated as ISE. The usual trend of the ISE is that the microhardness decreases with an increasing applied test load or an increasing indentation size. Recently, it has been shown that, phenomenologically, the ISE can be described by the proportional specimen resistance (PSR) [1, 2]. The PSR model has demonstrated a wide applicability to describe the ISE which has been observed in microhardness measurements for ceramics [3, 4], glasses [5], metals [2] and single-crystal diamond [6]. Utilization of the PSR model yields the indentation load-independent microhardness of the particular solid of interest.

An opposite or reverse form of the indentation size effect, RISE, has also been reported. As depicted in Fig. 1, the apparent microhardness increases with increasing applied indentation test load. The RISE has been reported in Vickers microhardness studies for several single crystals: Si(1 1 1), GaP(1 0 0), GaAs(1 1 1) and InP(1 0 0) [7]. The phenomenon has not been extensively studied, but several explanations have been advanced. For metallic materials, it may originate from the work hardening of the test specimen during the indentation loading. For brittle materials, however, it is common, for Vickers indentations, that specimen cracking occurs during the indentor loading half-cycle. Feltham and Banerjee [7, 8] have suggested that the RISE may be related to the energy loss as a result of specimen chipping surrounding the indentation during loading. Because of the cracking, a smaller indentation size results and the indentation test yields a higher apparent microhardness for a given applied test load. However, there is a lack of quantitative analysis relating the indentation-induced specimen cracking to the RISE. This paper establishes a physical basis to quantitatively analyse the previously published microhardness data for several single crystals exhibiting a RISE.

2. Indentation cracking effect on the microhardness

The microhardness is inversely proportional to the square of the indentation dimension, d^2, which makes any changes in the indentation size influenced by specimen cracking, significant. Fig. 2 illustrates the reported apparent Vickers microhardnesses as a function of indentation test load for single crystals of Si(1 1 1), GaAs(1 0 0), GaP(1 1 1) and InP(1 0 0) after Banerjee and Feltham [7]. For these measurements, different amounts of indentation-induced specimen cracking at different indentation test loads have been reported to exist [7]. It has been also reported that for silicon, one of the single-crystals measured, the critical load to initiate the indentation cracking is estimated to be only ~ 0.3 g [9] whereas the experimentally observed value is 3–5 g [10]. These previously reported values are less than the minimum indentation test loads for the measurements [7]. A natural question is whether the observed RISE, shown in Fig. 2, originates from the contribution of the indentation-induced cracking to the apparent Vickers microhardnesses of these four single crystals with similar structures.

If the Vickers microhardness values of Banerjee and Feltham [7] in Fig. 2 are closely considered, it is evident that an unusual phenomenon is dominating these measurements. This may not be so apparent from the InP and GaP results, but it is quite obvious

* Auhtor to whom correspondence should be addressed.

0022–2461

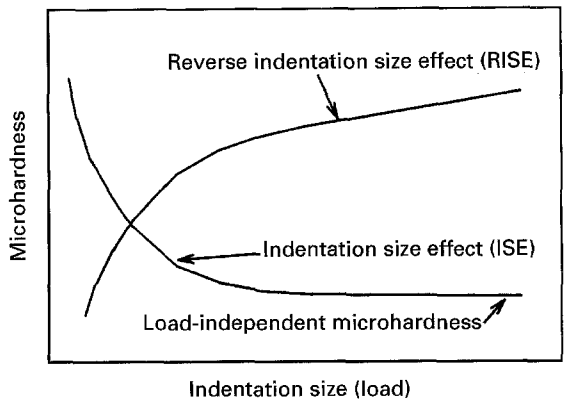

Figure 1 The normal and reverse forms of the indentation size (load) effect.

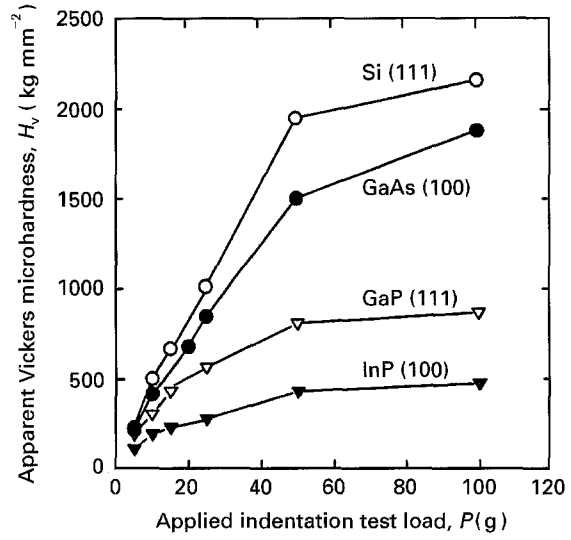

Figure 2 Indentation test load dependence of the Vickers microhardness of several single crystals after Banerjee and Feltham [7].

from the GaAs and silicon values. These latter two materials exhibit microhardnesses of nearly 2000 kg mm^{-2} or greater under the higher load levels. These values are more comparable to that of corundum (Al_2O_3) than to those for semiconductors, which might be expected to have hardnesses less than 1000 kg mm^{-2}. These comments are not meant to question the experimental results shown in Fig. 2, only to illustrate their unique character. As demonstrated in the following analysis and discussions, the excessively high microhardnesses exhibiting a RISE can be explained.

For a sharp pyramidal indentor, such as the Vickers, cracks are frequently generated when the specimen volume beneath the apex of the indentor is loaded. It is well known that median or radial cracks form primarily during the indentor loading half-cycle, while lateral cracks may form under the action of the residual stress field during the indentor unloading half-cycle [11, 12]. When addressing the issue of the effect of indentation cracking on the Vickers microhardness measurement, only those cracks created during the loading half-cycle are considered. This is because cracks created during the unloading half-cycle do not alter the resulting indentation dimensions related to plastic deformation of the test specimen.

Crack formation during the loading half-cycle releases some of the elastic strain energy in the test specimen and also increases the specimen compliance. Hence, it reduces the test specimen resistance to the indentor penetration. At the point of maximum penetration during the loading half-cycle, the applied indentation test load will be balanced by the total specimen resistance. This can be expressed as:

$$P = R_e + R_f + R_p + R_c \quad (1)$$

where P is the applied indentation test load, and the R terms are the individual specimen resistances: R_p relates to the plastic deformation, R_e to the elastic deformation, the friction at the indentor/specimen facet interface is R_f and the specimen cracking resistance is R_c, which is zero in the absence of specimen cracking. In the presence of indentation-induced cracking, the cracking resistance, R_c, is assumed to increase, becoming more important with an increase in the extent of cracking. Although Palmqvist cracks may be created during the loading half-cycle prior to the formation of the median crack, they are mainly confined near the subsurface of the test specimen. Because the critical load to initiate the median crack is less than the applied indentation test loads used [7, 9], the effects of Palmqvist cracks may be considered insignificant compared to the median cracks.

Fig. 3a(1) schematically depicts the indentation load, P, versus the indentation depth, h, for the case where indentation-induced cracking is present. Similar P–h curves have been observed in dynamic microhardness indentation measurement by Nowak *et al.* [13]. It clearly illustrates that during the loading half-cycle, specimen cracking created by the indentation process results in a series of abrupt indentor penetrations, or indentor sink-ins, somewhat analogous to crack pop-ins. The larger the indentation load, the greater is the number of the abrupt indentor sink-ins that will be observed and hence the greater their total penetration. The occurrence of specimen cracking increases the compliance of the test specimen, which can be treated as an equivalent reduction of the specimen's total resistance.

For the case when the indentation crack growth occurs in a stable fashion, accompanying indentor penetration [13], the process may be considered to be the superimposition of two separate steps: (i) shown in Fig. 3a(2), the indentor penetrates the specimen to the depth equal to ($h_p + h_e$), without specimen cracking, and (ii) the subsequent specimen cracking which allows an additional total amount of indentor penetration, Δh_c, as shown in Fig. 3a(3), which is a sum of each individual indentor sink-in. Fig. 3b illustrates the top view of a Vickers indentation, in which C is the radius of a fully developed median crack at the maximum indentation load, P_{max}, and d is the diagonal of the Vickers indentation.

According to Equation 1, specimen cracking reduces the elastic term, R_e, but increases the cracking resistance term, R_c, at the same time because the crack growth occurs in a quasi-equilibrium state. This force balance defines the driving force for the indentor

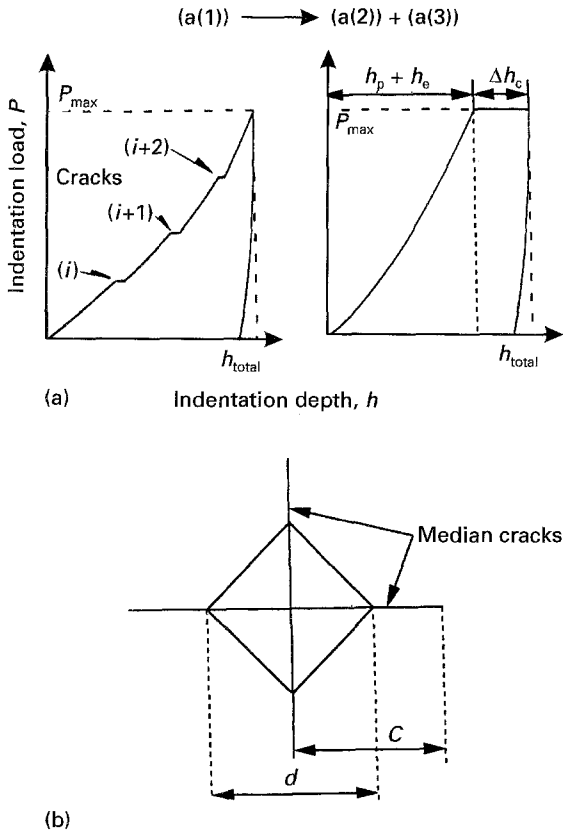

Figure 3 Indentation-induced cracking during loading Vickers microhardness measurements.

sink-ins. For the loading half-cycle and with the presence of indentation-induced cracking, the total indentation depth, h_{total}, is expressed as

$$h_{total} = h_p + h_e + \Delta h_c \quad (2)$$

The components of the specimen resistance, R_i, in Equation 1 can be related to the h_i contribution if weighted by a factor (h_i/h) where the subscript denotes each specific component in Equation 2. For a two-body contacting case, when the friction at the indentor/specimen surface is considered, an effective indentation test load, P_{eff}, is reduced to $(P - R_f)$. Hence each component of the specimen resistance may be described as

$$R_e = (h_e/h_{total})P_{eff} = (h_e/h)(P - R_f) \quad (3a)$$

$$R_p = (h_p/h_{total})P_{eff} = (h_p/h)(P - R_f) \quad (3b)$$

$$R_c = (\Delta h_c/h_{total})P_{eff} = (\Delta h_c/h)(P - R_f) \quad (3c)$$

the summation of which satisfies the force balance in Equation 1.

Considering the individual terms of Equations 3a and b, each component of resistance can be further described in its relationship to the indentation process as follows.

(i) Frictional component: upon normal loading, the contact surfaces will displace in opposite directions. The relative motion is restrained under the presence of the frictional traction at the indentor/specimen interface [14]. A simplified form of the friction may be

$$R_f = \mu\theta P \quad (4)$$

where μ is the coefficient of friction between the diamond indentor faces and the specimen indentation surface, and θ is a geometrical factor for the conversion of the applied indentation load to the loads normal to the contacting specimen surfaces.

(ii) Elastic component: the solution for a rigid cone in contact with a flat elastic specimen surface is of the form [15]

$$P = A_e h_e^2 = [E/2(1 - \nu^2)](\alpha_0/r_e^2)\tan\Psi h_e^2 \quad (5)$$

where E and ν are Young's modulus and Poisson's ratio of the test specimen, α_0 and Ψ are the geometric factors related to the geometry of indentor, and r_e and h_e are the geometric factor and the penetration depth related to the perfect elastic contribution of the test specimen, respectively. Substituting Equations 4 and 5 into Equation 3a, the elastic resistance of specimen is then

$$R_e = [E/2(1 - \nu^2)](1 - \mu\theta)(\alpha_0/r_e^2)\tan\Psi(h_e^3/h) \quad (6)$$

The elastic effects are quite complicated by the elastic anisotropy of single crystals. Thus, these effects will certainly have a strong orientation dependence, for the elastic constants, such as E and ν, are fourth-order tensors.

(iii) Plastic component: for a perfectly plastic body, the depth of indentation deformation can be related to the indentation test load as [16]

$$P = A_p h_p^2 = H_i(\alpha_0/r_p^2)\tan^2\Psi h_p^2 \quad (7)$$

where H_i is defined as the true microhardness of the material, which is a representative of a portion of the pure elastic deformation free from any forms of indentation artifacts, and r_p and h_p are the geometric factor and the penetration depth, respectively, which are related to the plastic contribution. Then, the substitution of Equations 4 and 7 into Equation 3b yields

$$R_p = (1 - \mu\theta)H_i(\alpha_0/r_p^2)\tan^2\Psi(h_p^3/h) \quad (8)$$

(iv) Specimen cracking component: in atomistic terms, a brittle crack grows by the sequential rupture of cohesive bonds across the crack plane, creating two new surfaces. The bond-rupture process operates under conditions of the thermodynamic (Griffith) equilibrium: energy release rate $(G) = 2\Gamma$ (surface energy, Γ). Once $G > 2\Gamma$, the crack propagates in a dynamic manner until the whole system, indentor and specimen, is under a newly defined equilibrium condition. For a median crack induced by a sharp indentor, such as a Vickers diamond, at the maximum indentation loading, that the equilibrium condition can be expressed in terms of the applied test load and the resulting crack dimension in the form [14]

$$P = (K_C/\chi_e)C^{3/2} \quad (9)$$

where C is the size of a fully propagated and stabilized median crack under the given loading condition, K_C is the stress intensity at the maximum indentation load, which may be related to the materials fracture toughness, and χ_e is a dimensionless indentor/specimen

constant, where the subscript e denotes the purely elastic stress field. Combining Equation 3c with Equations 4 and 9 yields

$$R_c = (1 - \mu\theta)(K_C/\chi_e)(C^{3/2}\Delta h_c/h) \quad (10a)$$

Assuming that Δh_c is proportional to the crack size, C, by a factor, ω [17], Equation 10a yields

$$R_c = (1 - \mu\theta)(\omega K_C/\chi_e)(C^{5/2}/h) \quad (10b)$$

Based on the force equilibrium at the maximum indentation test load, the apparent microhardness, H_{app}, can then be described according to the combination of Equations 1 and 2 as

$$H_{app} = \theta P/h^2 = \theta(R_e + R_p + R_c + R_f)/(h_e + h_p + \Delta h_c)^2 \quad (11)$$

The true microhardness, H_i, is related only to the irreversible plastic deformation [18]. By analogy to Equation 11, the true hardness is of the form $H_i = \theta R_p/h_p^2$. Equation 11 can then be rearranged to yield

$$H_{app} = \lambda H_i + \lambda_2(R_e + R_f + R_c) \quad (12)$$

where $\lambda_1 = (1 + h_e/h_p + \Delta h_c/h_p)^{-2}$, and $\lambda_2 = \theta/h^2$. From Equation 12, it is evident that there may exist several indentation-related artefacts which can increase the apparent microhardness to levels above and beyond the true microhardness. These are the elastic contribution, the frictional effect and also indentation-induced cracking. The net effect results in an apparent increase in the observed microhardness. From this format, it is possible to quantify the trends of the apparent microhardness as a function of the indentation test load, for there have appeared two exactly opposite indentation size/load effects as earlier discussed, the classical ISE and the RISE.

It has been recently demonstrated that for iron, which can be approximately treated as a perfectly plastic body, the effect of friction on the apparent microhardness is significant only for low indentation test loads. The influence of the friction between the indentor and the specimen facets results in a trend where the microhardness decreases with an increase in the applied indentation test load [19]. This trend exists for iron because the indentor/specimen contact area (the source of the friction) increases relative to the indentation volume as the test load (indentation size) decreases [2]. The elastic effect may be expected to lead to a similar trend for the indentation size effect [20]. Examination of those two factors suggests that the RISE, shown in Fig. 2, is not related to either the frictional effect or the elastic effect, otherwise the trend of a classical ISE would be observed. Clearly, it is not.

As only the indentation-induced cracking is expected to contribute to the RISE, it is appropriate to isolate and investigate cracking as a source for the phenomenon depicted in Fig. 1 and the experimental results illustrated in Fig. 2. Reducing Equation 12 to only the indentation cracking effect yields

$$H_{app} \cong \lambda_1 H_i + \lambda_2 R_c \quad (13)$$

Incorporating Equation 10b into Equation 13 gives:

$$H_{app} \cong \lambda_1 H_i + \lambda_2(1 - \mu\theta)(\omega K_C/\chi_e)(C^{5/2}/h) = \lambda_1 H_i + (1 - \mu\theta)(\theta\omega K_C/\chi_e)(C^{5/2}/h^3) \quad (14)$$

Based on the linear relation between the crack size, C, and the indentation test load, $P^{2/3}$, shown in Equation 9, the above equation can be rearranged to yield

$$H_{app} \cong \lambda_1 H_i + K[P^{5/3}/h^3] \quad (15)$$

where K is equal to $(1 - \mu\theta)\theta\omega K_C^{-2/3}\chi_e^{2/3}$. A peculiar (5/3) dependence of the apparent indentation microhardness on the applied indentation test load results. Nonetheless, it allows for the examination of the experimental results shown in Fig. 2. In Equation 15, for an ideally perfect plastic body, the apparent microhardness is equal to the true microhardness, and under this condition λ_1 is equal to unity. Because h_e and Δh_c are both equal to zero for that case, R_e and R_c vanish, too.

3. An application of the indentation-induced cracking (IIC) model

In Fig. 2, there obviously exists a general trend that the apparent microhardnesses increase with increasing indentation test load, the extent of which varies substantially for the four individual single crystals. To apply Equation 15 directly to those microhardness data which contain indentation-induced specimen cracking, it is most desirable to have directly monitored the indentation depth during loading to determine the precise indentation depth, h. However, for the data presented in Fig. 2, an estimation of the final indentation depth, h, using the indentation size after unloading, appears to be satisfactory. For example, the elastic recovery of the indentation size of an indentation which is measured immediately after unloading results in a slight underestimation of the indentation depth. When indentation cracking is present, this underestimation is reduced, for the specimen cracking releases a portion of the elastic strain energy stored in the specimen, which reduces the extent of elastic recovery. Furthermore, cracked indentations usually occur at high loads where the elastic contribution is not significant.

Table I summarizes the results of the Vickers microhardness and the calculated indentation size and estimated indentation depth as a function of the applied indentation test load, from which the quantity, $P^{5/3}/h^3$, in Equation 15 was determined, listed in Table I also. Fig. 4 illustrates the results of the application of the indentation-induced cracking model to the data from the four different single crystals shown in Fig. 2. In spite of the significant differences in microhardness levels, as well as the varying trends of microhardness–indentation load, it is evident that all of the results fall on a single curve. This confirms that the RISE is directly associated with the indentation-induced specimen cracking. It must be concluded that the RISE occurs because of indentation-induced cracking.

TABLE I Apparent Vickers microhardnesses and the application of the indentation-induced cracking model for several single crystals

		P(g) 5	10	15	20	25	50	100
Si (1 1 1)	H_v (kg mm^{-2})	231.6	502.0	670.4	–	1012.2	1947.9	2160.0
	d_{cal} (μm)	6.33	6.08	6.44	–	6.77	6.90	9.27
	h_{cal} (μm)	0.90	0.87	0.92	–	0.97	0.99	1.32
	$P^{5/3}/h^3$($g^{5/3}$ μm^{-3})	20.1	70.5	117.2	–	234.2	699.4	936.7
GaAs (1 0 0)	H_v (kg mm^{-2})	219.4	417.3	–	681.6	848.0	1503.0	1880.6
	d_{cal} (μm)	6.50	6.67	–	7.38	7.39	7.85	9.93
	h_{cal} (μm)	0.93	0.95	–	1.05	1.06	1.12	1.42
	$P^{5/3}/h^3$($g^{5/3}$ μm^{-3})	18.2	54.1	–	127.3	179.5	483.0	752.4
GaP (1 1 1)	H_v (kg mm^{-2})	193.9	305.1	432.6	–	564.3	809.2	868.4
	d_{cal} (μm)	6.92	7.80	8.02	–	9.06	10.70	14.61
	h_{cal} (μm)	0.99	1.11	1.15	–	1.29	1.53	2.09
	$P^{5/3}/h^3$($g^{5/3}$ μm^{-3})	15.1	33.9	60.0	–	99.6	189.5	236.0
InP (1 0 0)	H_v (kg mm^{-2})	115.3	194.9	231.6	–	278.6	430.6	473.5
	d_{cal} (μm)	8.97	9.75	10.96	–	12.90	14.67	19.79
	h_{cal} (μm)	1.28	1.39	1.57	–	1.84	2.10	2.83
	$P^{5/3}/h^3$($g^{5/3}$ μm^{-3})	7.0	17.3	23.6	–	34.3	73.3	95.1

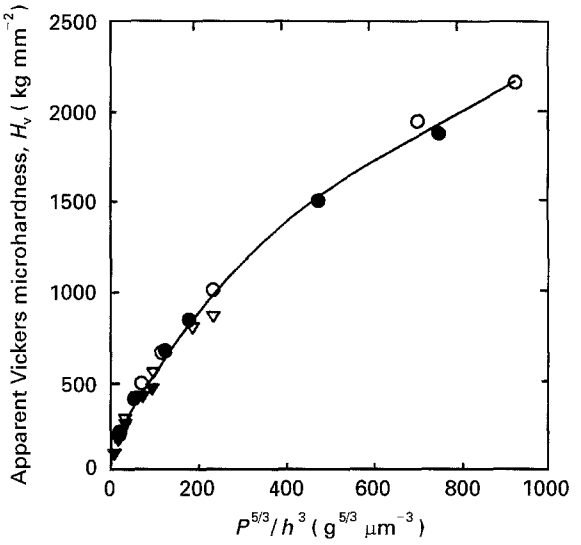

Figure 4 Analysis of the reverse indentation size effect (RISE) shown in Fig. 2 with the application of the indentation-induced cracking model. Single crystal: (○) Si (1 1 1); (●) GaAs (1 0 0); (▽) GaP (1 1 1); (▼) Inp (1 0 0).

The trend shown in Fig. 4 also reveals the non-linearity of Equation 15. This is related to the factor, ω, which is load-dependent. Dynamic microhardness measurements appear to be an appropriate means to investigate further the depth of indentor sink-in during the loading half-cycle and the median crack sizes as they are related to the indentation test load. For many microhardness measurements using a Vickers indentor, the indentation-induced cracking is inevitable. Combining the dynamic microhardness indentation method with the IIC model in a format of Equation 15, the true microhardness, H_i, can only be deduced from the intercept shown in Fig. 4. The parameter, λ_1, can be experimentally determined by measuring each individual contribution of the h_e and Δh_c over h_p, according to Equation 12.

4. Conclusion

The previously reported reverse form of the indentation size effect or RISE for Vickers microhardnesses of several single crystals with similar structure was addressed by considering the force equilibrium between the applied indentation test load and the test specimen resistance. An indentation-induced cracking model describing the RISE on the microhardness was developed and applied to previously published data. A well-defined relationship for the proposed mechanism and the previously published experimental data exists from which it is concluded that the RISE is caused by indentation-induced cracking.

Acknowledgements

The authors are grateful to Drs M. Sakai and M. Swain for making copies of manuscripts available to the authors. Discussions with Dr R. D. Sarno are acknowledged.

References

1. H. LI and R. C. BRADT, *J. Mater. Sci.* **28** (1993) 917.
2. H. LI, A. GHOSH, Y. H. HAN and R. C. BRADT, *J. Mater. Res.* **8** (1993) 1028.
3. H. LI and R. C. BRADT, *Mater. Sci. Eng.* **A142** (1991) 51.
4. *Idem, J. Hard Mater.* **3** (1992) 403.
5. *Idem, J. Non-Cryst. Solids* **146** (1992) 197.
6. *Idem, J. Diamond Rel. Mater.* **1** (1992) 1161.
7. P. FELTHAM and R. BANERJEE, *J. Mater. Sci.* **27** (1992) 1626.
8. R. BANERJEE and P. FELTHAM, *ibid.* **9** (1974) 1478.
9. B. R. LAWN and A. G. EVANS, *ibid.* **12** (1977) 2195.
10. J. LANKFORD and D. L. DAVIDSON, *ibid.* **14** (1979) 1662.
11. B. R. LAWN and M. V. SWAIN, *ibid.* **10** (1975) 113.
12. B. R. LAWN and E. R. FULLER, *ibid.* **10** (1975) 2016.
13. R. NOWAK, K. UENO and M. KINOSHITA, in "Fracture Mechanics of Ceramics, Vol. 10, edited by R. C. Bradt, D. P. H. Hasselman, D. Munz, M. Sakai and V. A. Shevchenko (Plenum Press, New York, 1992) p. 155.

14. R. B. LAWN and R. WILSHAW, *J. Mater. Sci.* **10** (1975) 1049.
15. I. N. SNEDDON, *Int. J. Eng. Sci.* **3** (1965) 47.
16. B. R. LAWN and V. R. HOWES, *J. Mater. Sci.* **16** (1981) 2745.
17. I. J. McCOLM, in "Ceramic Hardness" (Plenum Press, New York, 1990) Ch. 3, p. 145.
18. M. SAKAI, *Acta Metall. Mater.* **41** (1993) 1751.
19. M. ATKINSON and H. SHI, *Mater. Sci. Technol.* **5** (1989) 613.
20. D. R. TATE, *Trans. ASM* **35** (1945) 374.

Received 22 April 1994
and accepted 16 August 1995